Tuning color variation in grape anthocyanins at the molecular scale.

Laura Rustioni, Florent Di Meo, Maxime Guillame, Osvaldo Failla, Patrick Trouillas

HAL Id: inserm-00845052

https://inserm.hal.science/inserm-00845052

Submitted on 16 May 2014

Accepted Manuscript

Tuning Color Variation In Grape Anthocyanins At The Molecular Scale

Laura Rustioni, Florent Di Meo, Maxime Guillaume, Osvaldo Failla, Patrick Trouillas
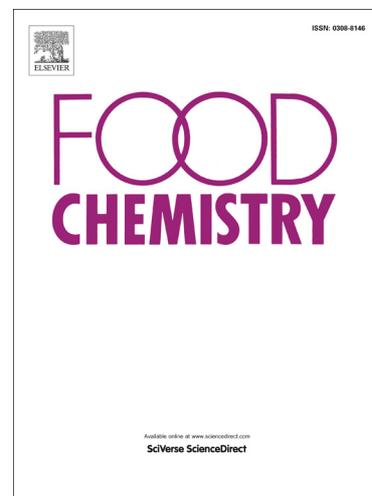
Please cite this article as: Rustioni, L., Di Meo, F., Guillaume, M., Failla, O., Trouillas, P., Tuning Color Variation In Grape Anthocyanins At The Molecular Scale, *Food Chemistry* (2013), doi: http://dx.doi.org/10.1016/j.foodchem. 2013.07.006

1 **Tuning Color Variation In Grape Anthocyanins At The Molecular Scale**

2 Laura Rustioni,[a,b,]* Florent Di Meo,[b] Maxime Guillaume,[c] Osvaldo Failla [a], Patrick

3 Trouillas[b,c,d]

4

5 [a] Università degli Studi di Milano, CIRIVE – Centro Interdipartimentale di ricerca per l'innovazione in

6 Viticoltura ed Enologia, via Celoria 2, I-20133 Milano, Italy

7 [b] Inserm, UMR-S850, Faculté de Pharmacie, Université de Limoges, 2 rue du Dr Marcland, 87000 Limoges,

8 France

9 [c] Laboratoire de Chimie des Matériaux Nouveaux, Université de Mons, Place du Parc, 20, B-7000, Mons,

10 Belgium

11 [d] Regional Center of Advanced Technologies and Materials, Department of Physical Chemistry, Faculty of

12 Science, Palacký University, 17. listopadu 1192/12, 77146 Olomouc, Czech Republic

13

14

15

16

17

18

19

20 **E-mail addresses:**

21 laura.rustioni@unimi.it, florent.di-meo@unilim.fr, maxime.guillaume@umons.ac.be ,

22 osvaldo.failla@unimi.it, patrick.trouillas@unilim.fr

23
24 **Corresponding author:**
25
26 Università degli Studi di Milano

27 CIRIVE Centro Interdipartimentale di ricerca per l'innovazione in Viticoltura ed Enologia

28 via Celoria 2

29 I-20133 Milano

30 ITALY

31 Tel.: +390250316556

32 Fax: +390250316553

33 E-mail: laura.rustioni@unimi.it

ABSTRACT

Anthocyanins are the main grape pigments. Due to their aromatic cyclic arrangements, they are able to absorb the radiation in the low energy range of the visible spectrum. In the fruit of *Vitis vinifera* L., the five main anthocyanidins (cyanidin, peonidin, delphinidin, petunidin and malvidin) are present as 3-*O*-glucosides, as well as their acetyl, *p*-coumaroyl and caffeoyl ester forms. Despite the huge number of experimental studies dedicated to the anthocyanin profile analysis of grapes and wines, the complete theoretical elucidation of the optical properties of grape anthocyanins is missing. The present work carried out this task through quantum chemistry calculations based on time-dependent density functional theory (TD-DFT), compared to experimental spectra. The differences in visible absorption spectra between the most common grape anthocyanins were rationalized according to B-ring substitution, glucosylation and esterification. A particular attention was given to the intra-molecular copigmentation effect, demonstrating the existence of an intra-molecular charge transfer excited state for the *p*-coumaroyl and caffeoyl ester forms.

52 **INTRODUCTION**

53 Anthocyanins are a class of π-conjugated compounds belonging to polyphenols. They are

54 glycosides of the so-called anthocyanidins, characterized by a flavylium (2-phenyl-

55 benzylpyrilium) skeleton (Fig. 1). The many possible chemical substitutions (with *e.g.*, OH

56 and OMe groups) allow a large variety of compounds. They are pigments responsible for the

57 shiny orange, pink, red, violet and blue colors in roots, stems, flowers and fruit of many plants

58 (*e.g.*, orchids, grapes) (Castañeda-Ovando, Pacheco-Hernández, Páez-Hernández, Rodríguez

59 & Galán-Vidal, 2009). Such a color variety is mainly driven by the capacity of these

60 compounds to absorb green light (at around 520 nm), which has generally been attributed to

61 the resonant structure of the flavylium cation (Allen, 1998; Castañeda-Ovando, et al., 2009).

62 This was confirmed by quantum chemistry calculations, showing a highly delocalized π-

63 conjugated system, spread over the entire molecule (Di Meo, Sancho Garcia, Dangles &

64 Trouillas, 2012). This extended π-conjugation allows light absorption in the visible range

65 rather than the violet to ultraviolet regions as it is described and theoretically rationalized for

66 most of the other natural polyphenols (Anouar, Gierschner, Duroux & Trouillas, 2012).

67 A thorough understanding of optical properties and pigmentation variation has become crucial

68 in various domains including food and wine chemistry. We believe that in a near future

69 fundamental rationalization of grape pigments should become mandatory to supporting the

70 development of fast and non-invasive phenotyping strategies (Rustioni, Basilico, Fiori, Leoni,

71 Maghradze & Failla, 2013). In grapes and wines, five anthocyanidin moieties are present in

72 their glucosylated form, namely peonidin, cyanidin, malvidin, petunidin and delphinidin (Fig.

73 1a). The most common anthocyanin in *Vitis vinifera* L. (*i.e.*, the common wine grape specie)

74 is malvidin-3-*O*-glucoside (Kennedy, Saucier & Glories, 2006). There also exist anthocyanins

75 having their glucose moiety attached to a carboxylic acid (acetic, *p*-coumaric and caffeic acids

76 in *Vitis vinifera* L.) by an ester bond, giving rise to a group of acylated pigments (Fig. 1b)

77 (Allen, 1998). In the latter structures, intra-molecular copigmentation effects have been

78 suggested (Dangles, Saito & Brouillard, 1993).

79   Despite all the available experimental studies focusing on the grape and wine anthocyanin

80 profiles (Dallas & Laureano, 1994; Ferrandino, Guidoni & Mannini, 2007; Fischer, Löchner

81 & Wolz, 2006; García-Puente Rivas, Alcalde-Eon, Santos-Buelga, Rivas-Gonzalo &

82 Escribano-Bailón, 2006; Mattivi, Guzzon, Vrhovsek, Stefanini & Velasco, 2006; Roggero,

83 Coen & Ragonnet, 1986; Rustioni, Rossoni, Calatroni & Failla, 2011; Rustioni, Rossoni,

84 Cola, Mariani & Failla, 2011; Rustioni, Rossoni, Failla & Scienza, 2013), a profound

85 understanding of the optical variability of these compounds is still missing. Quantum

86 chemistry calculation is an adapted tool for investigation of these properties. In particular time

87 dependent density functional theory (TD-DFT) enables to accurately characterize excited

88 states and evaluate the subsequent absorption properties in the visible range. More than

89 providing accurate absorption wavelengths, TD-DFT calculations provide a complete

90 description of the excited states and thus allow full assignment of electronic transitions from

91 the π to π^* molecular orbitals (MO) responsible for each UV/Vis absorption band. In this

92 way, the method supports the tuning of pigmentation in various industrial applications e.g.,

93 pigment painting and solar cells. Moreover the intra-molecular interactions suggested from

94 experience (Dangles, et al., 1993) can now be accurately evaluated by quantum calculations;

95 these interactions are known to be responsible for copigmentation, but the process was only

96 recently fully understood using dispersion-corrected DFT (DFT-D) calculations (Di Meo, et

97 al., 2012).

98   The present work aims at rationalizing the differences in the absorption spectra between a

99 series of grape anthocyanins, which has not been performed yet for these compounds. The

100 series studied here is constituted of five glucosylated (compounds **1-5** in Figure 1a) and three

101 acylated anthocyanins (compounds **6-8** in Figure 1b), which were investigated due to their

4

102 high occurrence in grape. This comprehensive study allows establishing a thorough structure-

103 property relationship for grape anthocyanins. In addition and as a new insight, the

104 copigmentation effects are carefully rationalized for the acylated anthocyanins.

105

106 **MATERIAL AND METHODS**

107 **Experimental data**

108 The grape anthocyanin spectra were collected from our database of HPLC chromatograms

109 obtained in 2008, within the framework of the study on competitive copigmentation

110 interactions (Rustioni, Bedgood Jr, Failla, Prenzler & Robards, 2012). Anthocyanins were

111 extracted from the skin of Shiraz and Sangiovese berries. The primary pigment solutions were

112 prepared after the careful removal of skin from 30 berries, and suspended in a 60 mL model-

113 wine-buffer solution (12% ethanol and 2.5 g L^{-1} tartaric acid adjusted at pH 3.3 with aqueous

114 NaOH). The pigment extracts were obtained by filtration after this mixture was shacked for 6

115 hours. The extracts were characterized on a Varian Prostar 240I HPLC (Mulgrave, Vic,

116 Australia) using a Phenomenex Gemini 5 μm C18 110A 250 x 4.6 mm column (Lane Cove,

117 NSW, Australia), with a Phenomenex SecurityGuard column, operated at 25°C. For the

118 HPLC separation the mobile phase was water:formic acid:acetonitrile (87:10:3 v/v/v, eluent

119 A; 40:10:50 v/v/v, eluent B), and the following gradient sequence was used: from 10 to 25%

120 B (10 min), from 25 to 31% B (5 min), from 31 to 40% B (5 min), from 40 to 50% B (10

121 min), from 50 to 100% B (10 min) from 100 to 10% B (5 min), as previously described by

122 Kammerer et al. (Kammerer, Claus, Carle & Schieber, 2004). The flow rate was 0.8 mL min^{-1}

123 ^{1}. The eluent was monitored by a Varian Prostar 335 photodiode array detector (Mulgrave,

124 Vic, Australia). Peak identification was achieved using both the retention time and the LCMS

125 analysis as previously described (Rustioni, et al., 2012).

5

126   Malvidin aglycone, and caffeic and *p*-coumaric acids (SIGMA-ALDRICH) were used

127   without further purification. To compare their spectra with those obtained in HPLC, three

128   solutions (10 mg L^{-1} for malvidin, 5.7 mg L^{-1} for caffeic acid and 3.2 mg L^{-1} for *p*-coumaric

129   acid) were prepared using the same solvent as for the HPLC elution (water:formic

130   acid:acetonitrile 65:10:25 v/v/v). A Jasco 7800 UV-Vis spectrophotometer was used to record

131   absorption spectra from 200 to 600 nm.

132   Considering the high percentage of formic acid providing pH ca. 1.6, the flavylium cation

133   form of the anthocyanins is unambiguously predominant. For this reason and for the sake of

134   comparison with experimental data, all the theoretical calculations were performed

135   considering this cationic form.

136

137   **Theoretical methodology**

138   Over the past decade, the density functional theory (DFT) has been validated and extensively

139   used to evaluate conformational, electronic and optical properties of natural polyphenols

140   (Anouar, Gierschner, Duroux & Trouillas, 2012; Trouillas, Marsal, Siri, Lazzaroni & Duroux,

141   2006). TD-DFT turned out to be an accurate theoretical method to describe excited states and

142   consequently UV/Visible properties at an acceptable computational time for medium-size

143   polyphenols, namely containing up to 200 atoms (Anouar, et al., 2012; Nave, et al., 2012).

144   Hybrid functionals succeeded at describing most of polyphenol properties; the B3P86

145   functional has appeared particularly adapted to assess both their thermodynamic (Trouillas, et

146   al., 2006) and UV/Visible absorption properties (Anouar, et al., 2012). Using the Pople-type

147   triple-ζ basis set, TD-B3P86/6-311+G(d,p) allowed to establish reliable structure property

148   (UV/Visible absorption) relationships for large series of polyphenols, at a reasonable

149   computational time (Anouar, et al., 2012; Millot, Di Meo, Tomasi, Boustie & Trouillas,

150   2012).

6

151   B3P86 was thus extrapolated for the present work to evaluate both conformation and

152   UV/Visible absorption properties of peonidin, cyanidin, malvidin, petunidin and delphinidin

153   and their glucoside derivatives (Fig. 1).

154   Concerning the acylated derivatives, cofacial (non-covalent) intra-molecular interactions

155   were examined between the anthocyanidin and the phenolic acyl (*i.e.*, *p*-coumaroyl and

156   caffeoyl) moieties. It is well described that classical hybrid functionals fail at describing these

157   non-covalent interactions, which are mainly dispersive effects (*e.g.*, π-stacking, ν-π and long-

158   distance H-bonds). The empirical dispersion-corrected DFT (DFT-D) is a successful approach

159   to evaluate these non-covalent complexation, also allowing to circumvent the use of high-

160   costing post-HF methods (Grimme, 2006). Our recent parameterization of the B3P86-D2

161   functional provided very reliable results to describe non-covalent interaction in polyphenols

162   and copigmentation (anthocyanidin:flavonol) complexes with respect to both post-HF

163   methods and experiments (Di Meo, et al., 2012). Therefore in the present work, the ground

164   state geometries of the acylated derivatives were corrected according to this empirical

165   dispersion correction. The cc-pVDZ basis set was used, which has appeared sufficient to

166   reach accuracy, with respect to high-level quantum calculations and experimental data, in the

167   description of anthocyanidin:flavonol complexation.[1] All DFT-D calculations were achieved

168   within the resolution of identity (RI) approximation, dramatically decreasing the

169   computational time with a negligible error (Neese, Wennmohs, Hansen & Becker, 2009).

170   When working with DFT-D(B3P86-D2), the geometries were obtained with the ORCA

171   package (Neese, 2012). In the other case i.e., when working with B3P86 (no dispersion

172   correction), the geometries were calculated with GAUSSIAN09 (Frisch, et al., 2009). All TD-

173   DFT calculations were achieved with GAUSSIAN09.

---

[1] It must be stressed that dispersion-corrected B3P86-D2 functional has been assessed and validated within double-z basis set precision.

174   Solvent effects were taken into account using implicit solvent models, in which the solute

175   is embedded in a shape-adapted cavity surrounded by a dielectric continuum. Even if they do

176   not explicitly account for inter-molecular interaction between solute and solvent, implicit

177   solvent models have allowed reaching accuracy to evaluate various properties of polyphenols,

178   including optical properties (Anouar, et al., 2012; Millot, et al., 2012). The qualitative

179   description of the influence of solvent polarity is particularly relevant, which perfectly

180   reproduce structure-property relationships. Methanol (ε = 32.61) was used to simulate the

181   polarity of the experimental conditions used to measure the UV/Visible spectra. The

182   conductor-like screening model (COSMO) (Sinnecker, Rajendran, Klamt, Diedenhofen &

183   Neese, 2006) and the integral-equation formalism polarizable continuum model (IEFPCM)

184   (Cossi, Scalmani, Rega & Barone, 2002) were used with ORCA and GAUSSIAN09,

185   respectively.

186

187   **RESULTS AND DISCUSSION**

188   **UV/Visible absorption properties of grape 3-*O*-glucosylated anthocyanins**

189   The experimental spectra measured for the five 3-*O*-glucosylated anthocyanidins

190   (compounds **1**-**5** namely cyanidin 3-*O*-glucoside, peonidin 3-*O*-glucoside, delphinidin 3-*O*-

191   glucoside, petunidin 3-*O*-glucoside and malvidin 3-*O*-glucoside – also called oenin – as seen

192   in Fig. 1), synthesized in grape berries, consist of three main peaks experimentally located at

193   around i) 520 nm (Band I), ii) 440 nm (Band II) and iii) 330 nm (Band III) (Fig. 2a). The di-

194   substituted B-ring compounds (*i.e.*, cyanidin 3-*O*-glucoside and peonidin 3-*O*-glucosides)

195   have an additional absorption band located at around 375 nm (Band II$_b$).

196

197   *Molecular orbital rationalization of Band I* - The highest absorption wavelength λ_{max}

198   corresponding to Band I of compounds **1**-**5** are 516, 517, 524, 526 and 527 nm, respectively

199 (Table 1). As already described for anthocyanidins, this wavelength is slightly underestimated

200 by TD-DFT calculations when using standard hybrid functionals (Anouar, et al., 2012; Chai

201 & Head-Gordon, 2008). This band corresponds to a transition from the ground state (S_0) to the

202 first excited state (S_1) and is mainly assigned to the HOMO (highest occupied molecular

203 orbital) to LUMO (lowest unoccupied molecular orbital) electronic transition.[2] In order to

204 simplify notations, the HOMO→LUMO electronic transition is quoted H→L throughout the

205 text. Both molecular orbitals (MO) are delocalized over the whole anthocyanidin moiety (Fig.

206 3a&b). This allows an efficient overlap between the two molecular orbitals involved in the

207 transition, which provides relatively high oscillator strengths (and therefore high absorption

208 intensities) for all five compounds (*f* around 0.60 as seen in Table 1).

209   The compounds having a tri-substituted B-ring (compounds **3**-**5**), exhibit a (red)-

210 bathochromic shift compared to the di-substituted (**1** and **2**) derivatives (Fig. 2a). This is

211 attributed to the (+M) mesomeric effect that slightly but significantly extends π-conjugation

212 in the B-ring, which subsequently lowered the H-L gap (ΔE_{gap}, Fig. 3a&b). When adding one

213 OH group (*i.e.*, compounds **1** *vs*. **3** and **2** *vs*. **4**), both H and L are stabilized but to a lower

214 extent for H, thus decreasing the gap (*e.g.*, ΔE_{gap} decreases from 2.91 to 2.86 eV, from **1** to **3**,

215 see Fig. 3a&b). Such an effect was similarly observed for aglycone flavonoids.(Anouar, et al.,

216 2012) When replacing an OH group by an OMe group, both frontier MOs are destabilized, but

217 the H orbital is more impacted by this destabilization, resulting in the decrease of the H-L gap

218 (*e.g.*, ΔE_{gap} is 2.86 and 2.75 eV for **3** and **5**, respectively, see S1).

219   The theoretical excited states of the aglycone counterpart of compounds **1**-**5** were also

220 evaluated for the sake of comparison. From this comparison, it appears that the sugar moiety

---

[2] In the present work, the orbital analysis is based on the 3D distribution of only the main two MO involved in the main electronic transition. The full analysis taking the contributions of all electronic transitions into account was also achieved (see Supplement Information). However, this latter (thorough) analysis does not influence the conclusions (except concerning one point, which is mentioned in the next footnote); thus for the sake of simplicity, the simpler analysis is kept in the main body of the text.

221   creates new MOs lying below H-4 (see Supplementary Information), which do not directly

222   influence the absorption spectra *e.g.*, by the formation of new bands. However, the sugar

223   addition induces a slight increase of the H-L gap, due to both the stabilization of H and

224   destabilization of L. This is in agreement with experimental data, as it results in a significant

225   hypsochromic shift of Band I in the glucosides' spectra (*e.g.*, λ_{max} equal 527 and 536 nm for

226   compound **5** and its aglycone counterpart, respectively as seen in Fig. 2b). This does not

227   influence the global spectra, which are similar in shape with both forms.

228   *Molecular orbital rationalization of Band II* - Band II appears in the experimental spectra

229   as a shoulder of the maximum absorption band, which is located at around 440 nm (Fig. 2a).

230   It corresponds to the second excited state (S_2) and is mainly assigned to the H-1→L and H-

231   2→L for di-substituted (*i.e.*, compounds **1** and **2**) and tri-substituted (*i.e.*, compounds **3-5**)

232   compounds, respectively (Table 1). L being delocalized on the A and C rings, this shoulder

233   appears attributed to this moiety. A thorough analysis of the MO spatial distribution

234   highlights interconversion between both H-1 and H-2 for the di- and tri-substituted

235   compounds; that is, the spatial distribution of H-1 in the di-substituted compound is similar to

236   that of H-2 in the tri-substituted compound (Fig. 3a&b). These MOs are delocalized over the

237   entire anthocyanidin moiety. Moreover, they exhibit the same energy (*ca*. -7.75 eV for all

238   compounds, as seen in Supplementary Information). For the tri- substituted compounds, H-1

239   is delocalized over the B-ring only. This MO slightly contributes to other excited states,

240   including S_1 (data not shown).

241   For the di-substituted compounds (**1** and **2**), there exists a specific absorption band, quoted

242   Band II$_b$ in Table 1, which is absent in the experimental spectra of the tri-substituted

243   compounds (**3**, **4** and **5**). Quantum chemistry calculations fully rationalize this experimentally

244   observed difference. Band II$_b$ is assigned to the H-2→L electronic transition. In the di-

245   substituted compounds, H-2 is slightly delocalized on the A&C-rings (Fig. 3a), allowing

246   electronic transitions with low oscillator strengths (f = 0.15 and 0.18 for **1** and **2**,

247   respectively). In the tri-substituted compounds, due to the MO redistribution described above,

248   H-1 is almost fully delocalized on the B-ring, preventing this electronic transition involving

249   the A&C-rings. Moreover, in this case, the energetic difference between H-1 and L is

250   lowered. Thus for the tri-substituted compounds, Band II_b is weak and red-shifted; it cannot

251   be experimentally observed under classical conditions (i.e., room temperature and classical

252   resolutions).

253

254   *Molecular orbital rationalization of Band III* - Band III is mainly assigned to the H-4→L

255   electronic transition. In agreement with the experimental data, Band III exhibits relatively low

256   oscillator strengths compare to those of Band I, for all five compounds (f is ranging from 0.02

257   to 0.08, see Table 1). The (blue)hypsochromic shift experimentally observed from the tri- to

258   the di-substituted compounds (*e.g.*, λ = 348 and 328 nm for **5** and **1**, respectively, see Table

259   1) is rationalized by the influence of the sugar moiety, which surprisingly, but in full

260   agreement with the experimental data, borrows part of the H-4 orbital, in the di-substituted

261   compounds (Fig. 3a&b). In this case the sugar moiety stabilizes H-4, thus increasing the

262   energy difference between H-4 and L, inducing the hypsochromic shift. This is probably only

263   an (energetic) indirect effect, as the electronic excitation does not involve the sugar moiety

264   (Fig. S2).[3]

265

266   **UV/Visible absorption properties of grape acylated anthocyanins**

267   The spectral modulation related to esterification is discussed for the malvidin derivatives,

268   as they are the main grape anthocyanidins.

269

---

[3] This is clearly observed when analyzing all MO involved in this electronic transition.

11

270   *Conformational analysis* - Concerning the three malvidin 3-*O*-glucoside esters

271   (compounds **6**, **7** and **8**, see Fig. 1) one, two (**7A** and **7B**) and two (**8A** and **8B**) conformers

272   were obtained, respectively (Fig. 4).

273   For each possible conformer, the Boltzmann distribution percentages D_{Bolt} were estimated

274   (Table 2) from the relative energies $\Delta E_{relative}$ (as calculated between all conformers with

275   B3P86-D2/cc-pVDZ), according to the following formula:

276
$$D_{Bolt} = \exp\left(-\frac{\Delta E_{relative}}{RT}\right),$$

277   where R is the ideal gas constant and T equals 298 K.

278   The non-covalent intra-molecular interactions between the acyl and anthocyanidin moieties

279   play a crucial role in the stabilization of these conformers. A strong H-bond (distance lower

280   than 1.65 Å) between the 5-OH and the ester keto groups is observed in **6**, **7B**, **8A** and **8B**

281   (Fig. 4). A weaker H-bond is observed between the 5-OH and the O atom involved in the

282   esterification (distance of 2.39 Å) for **7A**. Other non-covalent interactions are observed in **7A**,

283   **7B** and **8A** (Fig. 4), namely i) one H-bonding between the 7-OH and the 4″-OH groups

284   (distance of 1.80 and 2.27 Å, respectively) for **7A** and **7B**, which is not present in compound **8**

285   as 4″-OH is absent in this case, and ii) π-stacking interaction in **7B** and **8A** (distance of 4.20

286   Å).

287   The conformation populations of **7** and **8**, show a predominance of **7A** (D_{Bolt} = 90%) and

288   **8A** (D_{Bolt} = 83%) for both compounds, respectively. This clearly suggests that both H-bonding

289   and π-stacking interactions are the driving forces of this intra-molecular folding.

290

291   *UV/Visible absorption spectra of **6**, **7** and **8**: a matter of intra-molecular copigmentation* -

292   When compared to the glycosilated malvidin (**5**), the experimental spectra of **6**, **7** and **8**

293   clearly show the influence of esterification, mainly in the presence of the phenolic acid moiety

294   (compounds **7** and **8**). The three acylated anthocyanins exhibit an experimental bathochromic

295   shift of Band I that is lower for **6** ($\Delta\lambda max$ around 2, 5 and 4 nm for **6**, **7** and **8**, respectively).

296   The bathochromic shift of Band I is mainly rationalized by π-stacking complexation. In

297   conformations **7B** and **8A**, the maximum absorption wavelength (related to Band I) and other

298   very close absorption wavelengths are assigned to the H→L and H-1→L electronic transitions

299   (Table 2a). In all conformers, H and L are mainly delocalized on the anthocyanin moiety (Fig.

300   3c-f), and the electron transition presents no charge-transfer character. In the particular case of

301   conformers **7B** and **8A**, H is slightly located on the phenolic ring of the ester moiety (Fig.

302   3d&e). This can be better evaluated by the LCAO (linear combination of atomic orbital)

303   coefficients, which reflect the atomic weight of a given MO. For H of **7B** and **8A**, these

304   coefficients are 13% and 21% on the acyl moiety, respectively (Table S2). However, a

305   detailed analysis of MO contributions (see Supplementary Information) shows that the

306   esterification affects neither the spatial distribution nor the energy of H and L, showing that

307   the bathochromic shift is not rationalized by the H→L contribution. The main contribution to

308   the modification of the excited state (with respect to that of compound **5**) comes from H-1,

309   which is highly delocalized over the phenolic ester moiety for all conformers of **7** and **8** (Fig.

310   3c-f). Therefore the H-1→L electronic transition exists only because of the formation of a

311   charge transfer excited state (CT-ES), inducing a global bathochromic shift attributed to

312   esterification. In conformers **7B** and **8A**, H-1 is also located on the anthocyanin moiety (the

313   LCAO coefficients of H are 57% and 49% on the anthocyanin moiety, for **7B** and **8A**,

314   respectively see Table S2), which increases the corresponding oscillator strength (Table 2).

315   Compound **7** exhibits a slightly lower experimental bathochromic shift than **8** ($\Delta\lambda max$ = 4

316   and 5 nm, for both compounds respectively, see Table 2a). In contrast, the theoretical

317   bathochromic shift is higher with the former compound (**7**) i.e., 24.7 *vs.* 18.9 nm, for both

318   compounds respectively (Table 2a). This is consistent with the higher electron donor capacity

319   of the ortho-dihydroxyphenyl (catechol) moiety. Thus the lower experimental bathochromic

320   shift observed for **7** is attributed to a lower population of the π-stacked conformation (**7B**) in

321   solution compared to that of **8** (**8A**). This highlights the importance of i) charge-transfer in the

322   excited state and ii) populations for all the possible copigmentation complexes, as already

323   shown in our previous work (Di Meo, et al., 2012).

324

325   *A new band (III$_b$) at 330 nm* - The acylated compounds exhibit a new absorption band,

326   quoted Band III$_b$, experimentally located at around 330 nm (Fig. 2c), which is somehow a

327   modulation of Band III. This band is actually the sum of the minor anthocyanic absorption

328   Band III (Table 1 and Fig. 2a) and the (red)bathochromic-shifted band mainly attributed to the

329   stand-alone phenolic acid (*e.g.*, λ = 324 and 336 nm for caffeic acid and the caffeoyl ester of

330   malvidin 3-*O*-glucoside, respectively and λ = 309.6 and 316 nm for *p*-coumaric acid and the

331   *p*-coumaroyl ester of malvidin 3-*O*-glucoside, respectively, see Table 2b and Fig. 2c). It is

332   theoretically assigned to several contributions predominantly H-1$\rightarrow$L+1, H-4/5/6$\rightarrow$L and

333   H$\rightarrow$L+2 electronic transitions (Table 2b). The first contribution is purely attributed to the

334   phenol acid moiety, both MO being delocalized on this moiety. These MO are stabilized in

335   the presence of the anthocyanin moiety, H being more stabilized than L, which should induce

336   a hypsochromic shift. The global bathochromic shift is due to the other two contributions.

337   Among these contributions, the H-4$\rightarrow$L contribution corresponds to that already observed for

338   compound **5**, as the main contribution of Band III.

339

340   **CONCLUSION**

341   Grapes and wines represent agricultural product of utmost importance in food industry.

342   The color of the final product is a major descriptor of quality. A deep understanding of the

343   optical properties of the main *Vitis vinifera* L. pigments represents an effective support for the

344   industries to address market requirements. This is mandatory to develop new analytical

345   methods based on the optical properties and to deeply understand fruit potential. As described

346   above, quantum chemistry calculations have allowed elucidating the structure (optical)

347   properties of a series of grape pigments. These calculations provide a molecular picture of the

348   pigments as well as a molecular orbital description of the excited states related to the different

349   absorption bands responsible for color. Subtle effects such as copigmentation can also be

350   explained by using the adapted theoretical methodologies, namely DFT-D. All the theoretical

351   data support the experimental observations. The full MO description of light absorption, in the

352   visible range, enables to tune optical properties (according to the chemical structures of the

353   different grape pigments), and subsequently color variation. Quantum calculation can now be

354   considered as a promising analytical tool for wine industry.

370 **TABLES**

371 **Table 1.** Theoretical excitation energies (E, eV), absorption wavelengths (λ, nm), oscillator
372 strengths (*f*), main electronic transition contribution and experimental absorption wavelength
373 (λ_{exp}, nm) of anthocyanidin 3-*O*-glucosides. The calculations (excited states + geometries)
374 were performed with IEFPCM-B3P86/6-311+G(d,p).
375

Band	Compound	E	λ	f	Electronic transition contribution	λ_{exp}
I	**1**	2.59	478.0	0.58	H→L (67%)	516
	2	2.57	482.8	0.59	H→L (68%)	517
	3	2.57	482.8	0.57	H→L (67%)	524
	4	2.56	483.4	0.61	H→L (68%)	526
	5	2.49	497.1	0.59	H→L (68%)	527
II	**1**	2.95	419.8	0.07	H-1→L (67%)	~440
	2	2.92	424.8	0.03	H-1→L (68%)	~440
	3	2.95	420.1	0.11	H-2→L (67%)	~440
	4	2.93	423.7	0.06	H-2→L (67%)	~440
	5	2.92	424.0	0.05	H-2→L (68%)	~440
II$_b$	**1**	3.23	384.0	0.15	H-2→L (70%)	373
	2	3.22	385.2	0.18	H-2→L (69%)	375
	3	2.68	463.2	0.03	H-1→L (70%)	-
	4	2.70	456.0	0.01	H-1→L (70%)	-
	5	2.68	461.9	0.07	H-1→L (70%)	-
III	**1**	3.88	319.5	0.02	H-4→L (62%)	328
	2	3.88	319.8	0.02	H-4→L (62%)	328
	3	3.73	332.2	0.06	H-4→L (66%)	346
	4	3.72	332.9	0.08	H-4→L (66%)	347
	5	3.69	336.2	0.08	H-4→L (66%)	348

376

17

377 **Table 2.** Theoretical excitation energies (E, eV), absorption wavelengths (λ, nm), oscillator
378 strengths (*f*), electronic transition contribution and experimental absorption wavelength (λ*exp*,
379 nm) of the different optimized conformation of acetyl (**6**), caffeyl (**7**) and *p*-coumaryl (**8**)
380 esters of malvidin 3-*O*-glucoside, and related theoretical and experimental bathochromic
381 shifts (Δλ*th* and Δλ*exp*, nm) concerning (a) Band I and (b) Band III. Boltzmann
382 distributions D_{Boltz} are expressed in %. The calculations were performed with IEFPCM-
383 B3P86/6-311+G(d,p)//COSMO-B3P86(D2)/cc-pVDZ.

384 (a)

Ester	Conformation	D_{Boltz}	E	λ	*f*	Electronic transition contribution	Δλ*th* [a]	Exp	
								λ*exp*	Δλ*exp* [a]
Acetic ester	**6**	90%	2.51	494.9	0.58	H→L (68%)	-2.2	529	2
Caffeoyl ester	**7A**	90%	2.47	502.2	0.17	H-1→L (57%)	5.0	531	4
						H→L (40%)			
			2.50	496.5	0.38	H→L (54%)	-0.6		
	7B	6%	2.38	521.8	0.10	H-1→L (52%)	24.7		
			2.49	498.1	0.37	H-1→L (46%)	1.0		
						H→L (49%)			
p-Coumaroyl ester	**8A**	83%	2.40	516.0	0.41	H→L (66%)	18.9	532	5
			2.59	479.5	0.03	H-1→L (58%)			
	8B	15%	2.50	495.2	0.57	H→L (67%)	-1.9		

385 *[a] the shift is performed with respect to malvidin 3-O-glucoside λ*max*.*

386 (b)

Ester	Conformation	D_{boltz}	E	λ	*f*	Electronic transition contribution	Δλ*th*	Exp	
								λ*exp*	Δλexp
Acetic ester	**6**	100	3.64	340.8	0.07	H-3→L (65%)	nd	348	nd
Caffeoyl ester	**7A**	90%	3.66	339.1	0.03	H-5→L (48%)	1.1	324	12
						H-6→L (36%)			
						H-1→L+1 (31%)			
						H→L+2 (15%)			
			3.72	333.5	0.64	H-1→L+1 (62%)	-4.5		
	7B	6%	3.51	353.7	0.32	H-1→L+1 (68%)	15.7		
						H-4→L+1 (10%)			
			3.64	340.5	0.03	H-5→L (65%)	2.5		
p-Coumaroyl ester	**8A**	83%	3.68	336.6	0.25	H-1→L+1 (55%)	19.6	316	6
						H-5→L (33%)			
			3.74	331.5	0.22	H-5→L (47%)	14.5		
						H-1→L+1 (34%)			
						H→L+2 (15%)			
	8B	15%	3.70	334.8	0.68	H-1→L+1 (64%)	17.7		
						H-4→L+(14%)			
			3.75	331.1	0.13	H-6→L (62%)	14.0		
						H-4→L (20%)			
						H-1→L+1 (19%)			
						H-6→L (15%)			

18

387 ^{a} *the shift is performed with respect to the stand-alone acid* λ_{max} *(i.e., caffeic or p-coumaric acid in solution).*

388   **REFERENCES**

389   Allen, M. (1998). Phenolics and Extraction. In A. S. o. V. a. Oenology (Ed.), *Proceedings*

390   *ASVO*, Accepted). Adelaide.

391   Anouar, E. H., Gierschner, J., Duroux, J.-L., & Trouillas, P. (2012). UV/Visible spectra of

392   natural polyphenols: A time-dependent density functional theory study. *Food Chemistry,*

393   *131*, 79-89.

394   Castañeda-Ovando, A., Pacheco-Hernández, M. d. L., Páez-Hernández, M. E., Rodríguez,

395   J. A., & Galán-Vidal, C. A. (2009). Chemical studies of anthocyanins: A review. *Food*

396   *Chemistry, 113*, 859-871.

397   Chai, J.-D., & Head-Gordon, M. (2008). Long-range corrected hybrid density functionals

398   with damped atom-atom dispersion corrections. *Physical Chemistry Chemical Physics, 10*,

399   6615-6620.

400   Cossi, M., Scalmani, G., Rega, N., & Barone, V. (2002). New developments in the

401   polarizable continuum model for quantum mechanical and classical calculations on

402   molecules in solution. *Journal of Chemical Physics, 117*, 43-54.

403   Dallas, C., & Laureano, O. (1994). Effect of SO2 on the extraction of individual

404   anthocyanins and colored matter of three Portuguese grape varieties during winemaking.

405   *Vitis*, Accepted.

406   Dangles, O., Saito, N., & Brouillard, R. (1993). Anthocyanin intramolecular copigment

407   effect. *Phytochemistry, 34*, 119-124.

408   Di Meo, F., Sancho Garcia, J. C., Dangles, O., & Trouillas, P. (2012). Highlights on

409   Anthocyanin Pigmentation and Copigmentation: A Matter of Flavonoid π-Stacking

410   Complexation To Be Described by DFT-D. *Journal of Chemical Theory and Computation,*

411   *8*, 2034-2043.

412   Ferrandino, A., Guidoni, S., & Mannini, F. (2007). Grape quality parameters and

413   polyphenolic content of different 'Barbera' and 'Nebbiolo' (Vitis vinifera L.) clones as

414   influenced by environmental conditions – preliminary results. *Acta Horticulturae, 754*,

415   437-442.

416   Fischer, U., Löchner, M., & Wolz, S. (2006). Red Wine Authenticity: Impact of

417   Technology on Anthocyanin Composition. In *Authentication of Food and Wine*, vol. 952

418   (pp. 239-253): American Chemical Society.

419   Frisch, M. J., Trucks, G. W., Schlegel, H. B., Scuseria, G. E., Robb, M. A., Cheeseman, J.

420   R., Scalmani, G., Barone, V., Mennucci, B., Petersson, G. A., Nakatsuji, H., Caricato, M.,

421   Li, X., Hratchian, H. P., Izmaylov, A. F., Bloino, J., Zheng, G., Sonnenberg, J. L., Hada,

422   M., Ehara, M., Toyota, K., Fukuda, R., Hasegawa, J., Ishida, M., Nakajima, T., Honda, Y.,

423   Kitao, O., Nakai, H., Vreven, T., Montgomery, J. A., Peralta, J. E., Ogliaro, F., Bearpark,

424   M., Heyd, J. J., Brothers, E., Kudin, K. N., Staroverov, V. N., Kobayashi, R., Normand, J.,

425   Raghavachari, K., Rendell, A., Burant, J. C., Iyengar, S. S., Tomasi, J., Cossi, M., Rega,

426   N., Millam, J. M., Klene, M., Knox, J. E., Cross, J. B., Bakken, V., Adamo, C., Jaramillo,

427   J., Gomperts, R., Stratmann, R. E., Yazyev, O., Austin, A. J., Cammi, R., Pomelli, C.,

428   Ochterski, J. W., Martin, R. L., Morokuma, K., Zakrzewski, V. G., Voth, G. A., Salvador,

429   P., Dannenberg, J. J., Dapprich, S., Daniels, A. D., Farkas, Foresman, J. B., Ortiz, J. V.,

430   Cioslowski, J., & Fox, D. J. (2009). Gaussian 09, Revision A.02. In*, citeulike-article-

431   id:9096580). Wallingford CT.

432   García-Puente Rivas, E., Alcalde-Eon, C., Santos-Buelga, C., Rivas-Gonzalo, J. C., &

433   Escribano-Bailón, M. T. (2006). Behaviour and characterisation of the colour during red

434   wine making and maturation. *Analytica Chimica Acta, 563*, 215-222.

435   Grimme, S. (2006). Semiempirical GGA-type density functional constructed with a long-

436   range dispersion correction. *Journal of Computational Chemistry, 27*, 1787-1799.

437   Kammerer, D., Claus, A., Carle, R., & Schieber, A. (2004). Polyphenol Screening of

438   Pomace from Red and White Grape Varieties (Vitis vinifera L.) by HPLC-DAD-MS/MS.

439   *Journal of Agricultural and Food Chemistry, 52*, 4360-4367.

440   Kennedy, J. A., Saucier, C., & Glories, Y. (2006). Grape and Wine Phenolics: History and

441   Perspective. *American Journal of Enology and Viticulture, 57*, 239-248.

442   Mattivi, F., Guzzon, R., Vrhovsek, U., Stefanini, M., & Velasco, R. (2006). Metabolite

443   Profiling of Grape: Flavonols and Anthocyanins. *Journal of Agricultural and Food*

444   *Chemistry, 54*, 7692-7702.

445   Millot, M., Di Meo, F., Tomasi, S., Boustie, J., & Trouillas, P. (2012). Photoprotective

446   capacities of lichen metabolites: A joint theoretical and experimental study. *Journal of*

447   *Photochemistry and Photobiology B: Biology, 111*, 17-26.

448   Nave, F., Bràs, N. F., Cruz, L., Teixeira, N., Mateus, N., Galembeck, S. E., Di Meo, F.,

449   Trouillas, P., Dangles, O., & De Freitas, V. (2012). The influence of a flavan-3-olic

450   substituent in the copigmentation ability of anthocyanins towards vinylcatechin dimers and

451   procyanidins. *Journal of Physical Chemistry B, 116*, 14089-14099.

452   Neese, F. (2012). The ORCA program system. *Wiley Interdisciplinary Reviews:*

453   *Computational Molecular Science, 2*, 73-78.

454   Neese, F., Wennmohs, F., Hansen, A., & Becker, U. (2009). Efficient, approximate and

455   parallel Hartree-Fock and hybrid DFT calculations. A 'chain-of-spheres' algorithm for the

456   Hartree-Fock exchange. *Chemical Physics, 356*, 98-109.

457   Roggero, J. P., Coen, S., & Ragonnet, B. (1986). High Performance Liquid

458   Chromatography Survey on Changes in Pigment Content in Ripening Grapes of Syrah. An

459   Approach to Anthocyanin Metabolism. *American Journal of Enology and Viticulture, 37*,

460   77-83.

461   Rustioni, L., Basilico, R., Fiori, S., Leoni, A., Maghradze, D., & Failla, O. (2013). Grape

462   Colour Phenotyping: Develpment of a Method Based on the Reflectance Spectrum.

463   *Phytochemical Analysis,* 10.1002/pca.2434.

464   Rustioni, L., Bedgood Jr, D. R., Failla, O., Prenzler, P. D., & Robards, K. (2012).

465   Copigmentation and anti-copigmentation in grape extracts studied by spectrophotometry

466   and post-column-reaction HPLC. *Food Chemistry, 132*, 2194-2201.

467   Rustioni, L., Rossoni, M., Calatroni, M., & Failla, O. (2011). Influence of bunch exposure

468   on anthocyanins extractability from grapes skins (*Vitis vinifera* L.). *Vitis, 50*, 137-143.

469   Rustioni, L., Rossoni, M., Cola, G., Mariani, L., & Failla, O. (2011). Bunch exposure to

470   direct solar radiation increases ortho-diphenol anthocyanins in Northern Italy climatic

471   condition. *Journal Internation des Sciences de la Vigne et du Vin, 45*, 85-99.

472   Rustioni, L., Rossoni, M., Failla, O., & Scienza, A. (2013). Anthocyanin esterification in

473   Sangiovese grapes. *Italian Journal of Food Science, 25*, 133-141.

474   Sinnecker, S., Rajendran, A., Klamt, A., Diedenhofen, M., & Neese, F. (2006). Calculation

475   of Solvent Shifts on Electronic g-Tensors with the Conductor-Like Screening Model

476   (COSMO) and Its Self-Consistent Generalization to Real Solvents (Direct COSMO-RS).

477   *Journal of Physical Chemistry A, 110*, 2235-2245.

478   Trouillas, P., Marsal, P., Siri, D., Lazzaroni, R., & Duroux, J. L. (2006). A DFT study of

479   the reactivity of OH groups in quercetin and taxifolin antioxydants : The specificity of the

480   3-OH site. *Food Chemistry, 97*, 10.

481

482

23

483   **FIGURE CAPTIONS**

484

485   **Figure 1.** Chemical structures of the five glucosylated (a) and three acylated (b) studied

486   anthocyanins.

487

488   **Figure 2.** Experimental spectra of (a) anthocyanidin 3-*O*-glucosides (compounds **1-5**); (b)

489   malvidin aglycone and malvidin 3-*O*-glucoside (**5**); and (c) malvidin 3-*O*-glucoside (**5**), oenin

490   esters (compounds **7** and **8**), and relative phenolic acids.

491   All the spectra are normalized to appear in at a similar scale: anthocyanic molecules are

492   normalized at a relative absorption value of 100 in the main peak (ca. 530 nm); phenolic acids

493   are normalized according to the corresponding ester (ca. 330 nm).

494

495   **Figure 3.** Molecular orbital (MO) diagrams of the di-substituted (a) compound **1** and (b) tri-

496   substituted compound **3** and the different conformations of compounds **7** and **8**: (c) **7A** (d) **7B**,

497   (e) **8A** and (f) **8B**. The anthocyanidin moiety is in red, the sugar moiety is in blue and the acyl

498   moiety is in green. The calculations were performed with IEFPCM-B3P86/6-311+G(d,p) and

499   IEFPCM-B3P86/6-311+G(d,p)//COSMO-B3P86(D2)/cc-pVDZ   with   **1&3**   and   **7&8**,

500   respectively.

501

502   **Figure 4.** Optimized geometries of the acetyl ester (**6**), caffeic ester (**7A; 7B**) and p-coumaric

503   ester (**8A; 8B**) of malvidin 3-*O*-glucoside; the anthocyanidin, sugar and the acyl moieties are

504   in red, blue and green, respectively. The most relevant non-covalent intra-molecular

505   interactions between the acyl and anthocyanidin moieties are underlined by broken lines. The
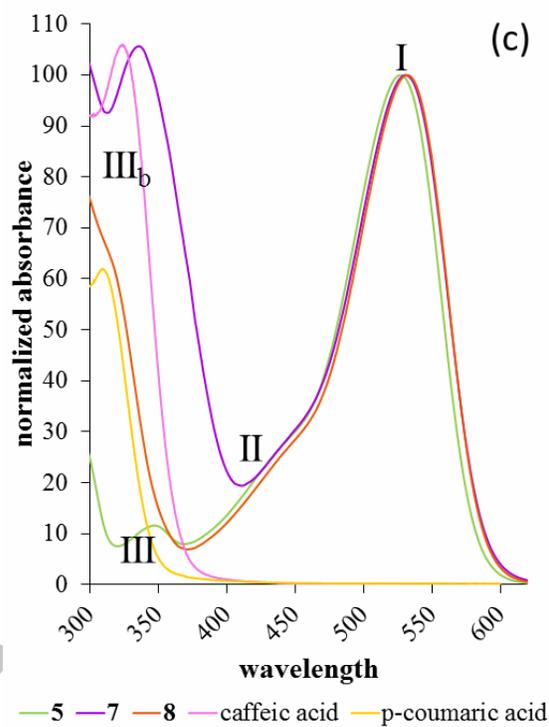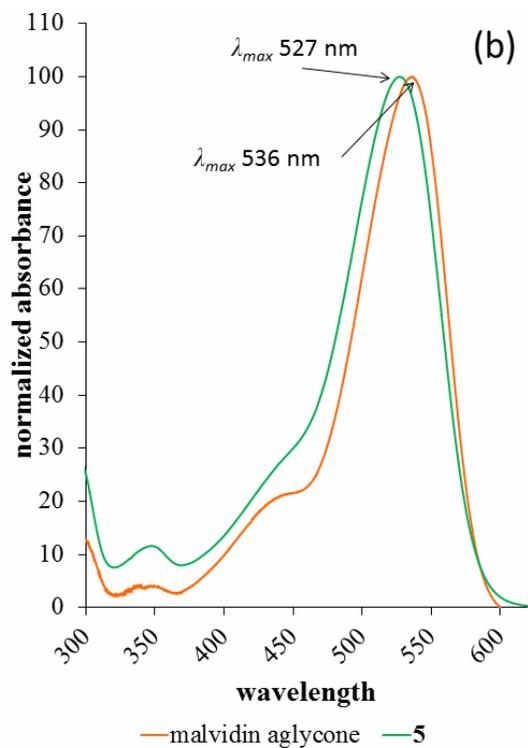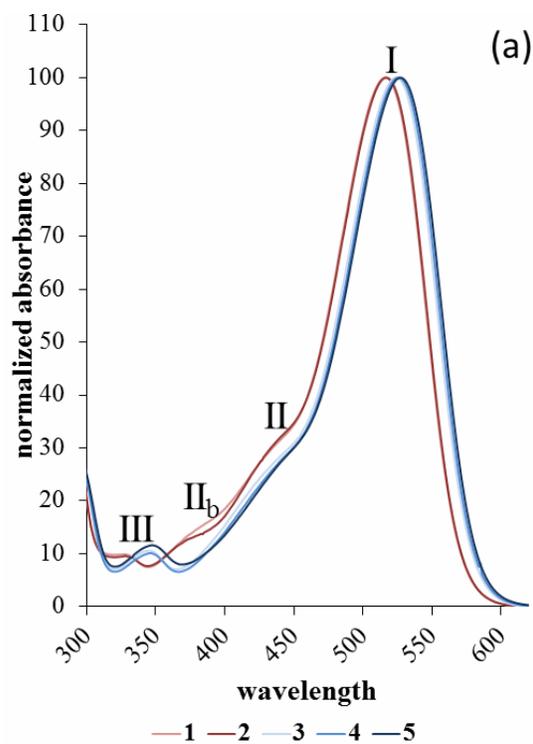
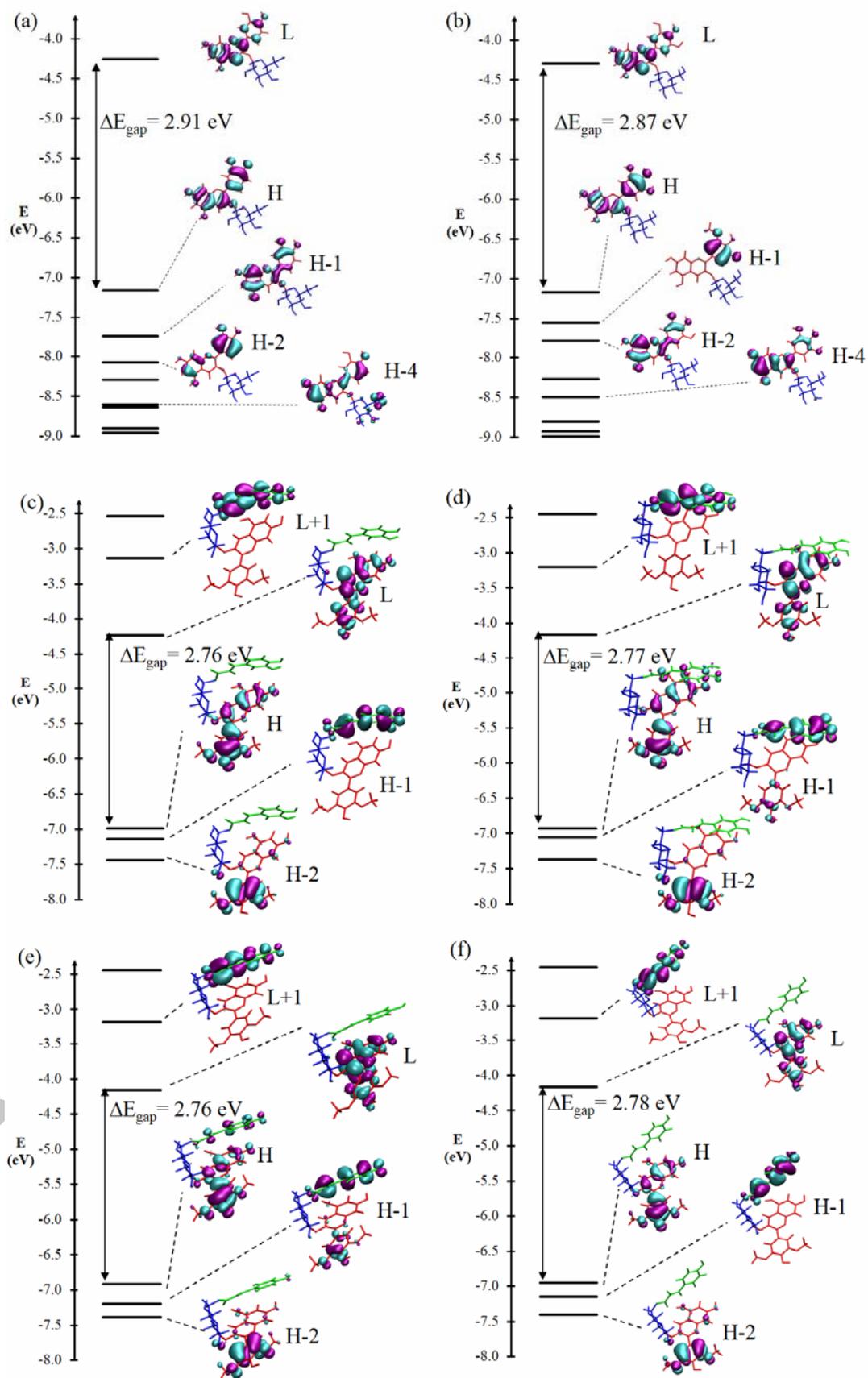506   calculations were performed with IEFPCM-B3P86/6-311+G(d,p)//COSMO-B3P86(D2)/cc-

507   pVDZ.

508

25

(a)

(b)

(c)
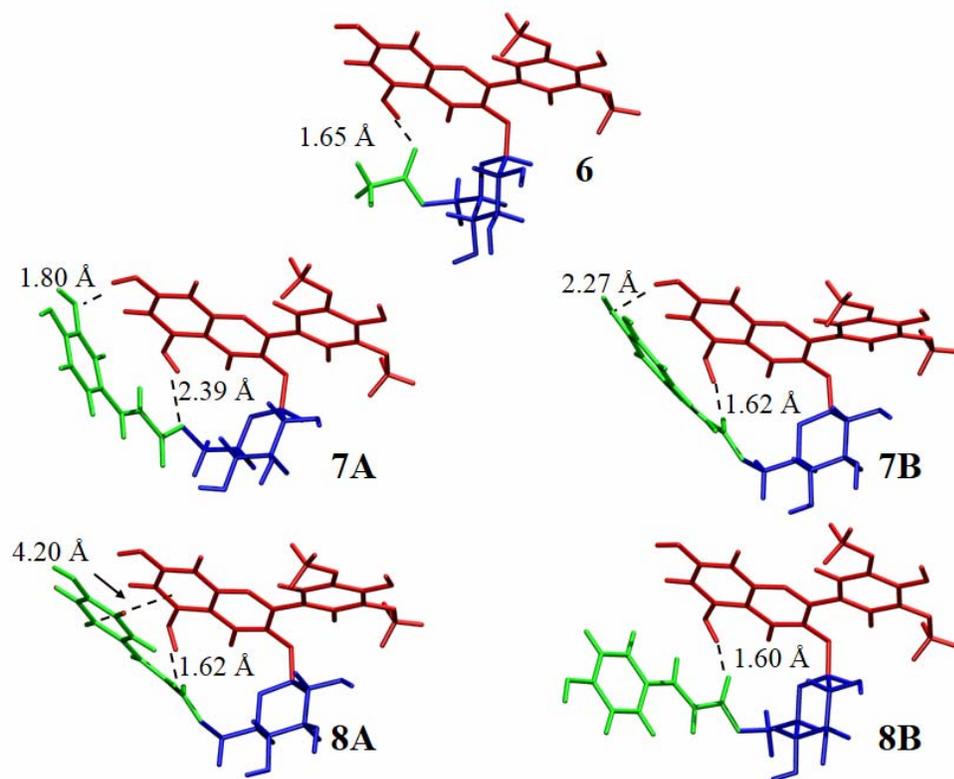
509

26

511

28
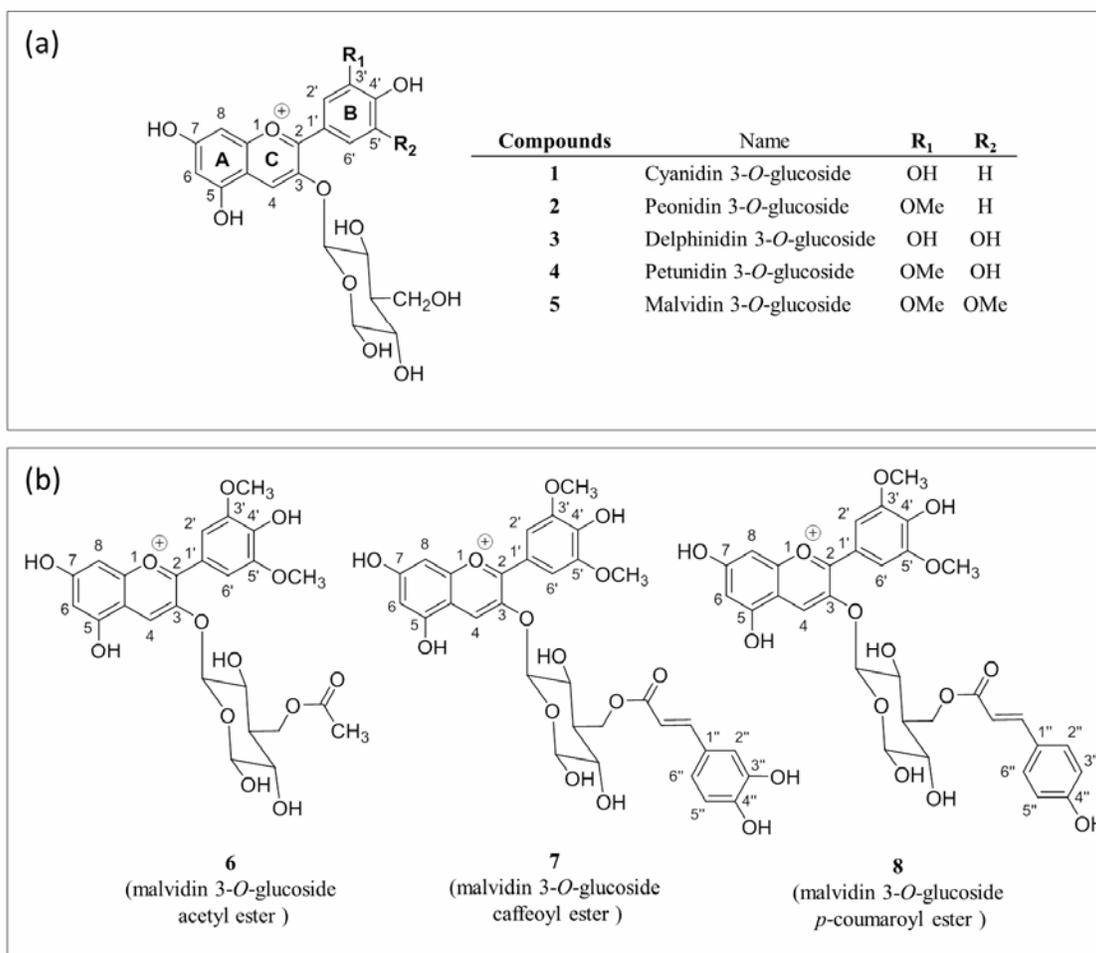
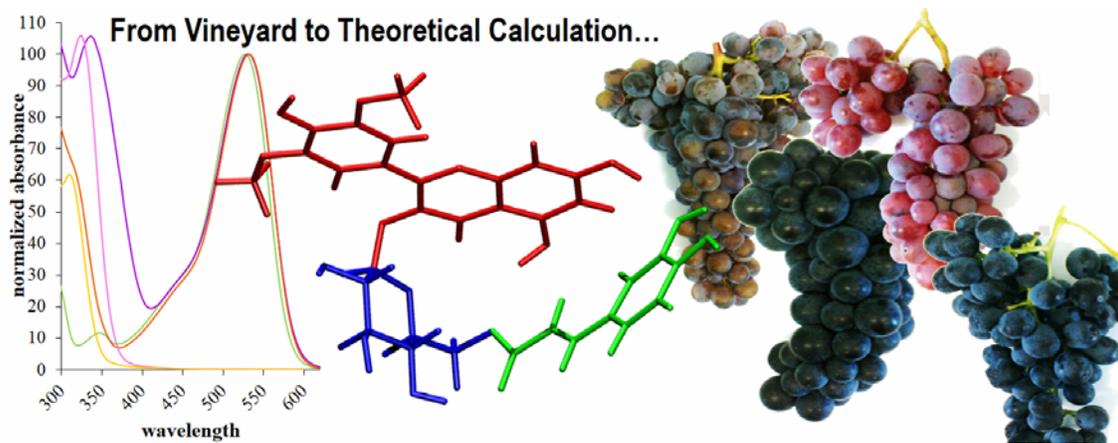512 **HIGHLIGHTS**:

513   Grape anthocyanins colors were rationalized using quantum chemistry calculations.

514   Absorption differences related to pigment substitutions were explained.

515   Intramolecular copigmentation was rationalized for acylated pigments.

516

517